Synthesis, spectroscopy and structural elucidation of two new Co^{II} and Ni^{II} complexes of pyrazole derived heterocyclic Schiff base ligand as potential anticancer and photocatalytic agents

Suman Mandal, Arka Bagchi, Arunima Biswas, David B. Cordes, Alexandra M.Z. Slawin, and Nitis Chandra Saha

Synthesis, Spectroscopy and Structural Elucidation of Two new Co^{II} and Ni^{II} Complexes of Pyrazole derived Heterocyclic Schiff base ligand as Potential Anticancer and Photocatalytic Agents

Abstract

Two new complexes **I** and **II** of general composition, $[ML_3]X_2.nH_2O$ (where, M = Co^{II} and Ni^{II} for **I** and **II**, respectively, L = MPAFA, X = Br and n = 2) were synthesized from a pyrazolyl Schiff base ligand, MPAFA (**L**). **I** and **II** were characterised through several physico-chemical and spectroscopic techniques, viz., C, H, N analyses, estimation of metal contents, conductance and magnetic susceptibility measurements, IR, electronic and fluorescence spectral studies. Both the reported coordination complexes were cationic in nature and behaved as 1:2 electrolytes. According to IR spectra, each of the MPAFA molecule coordinated to the metal centres via the azomethine nitrogen and the pyrazolyl tertiary nitrogen atoms. Single crystal X-ray diffraction studies of **I** and **II** had established a N_6 donor set with a distorted octahedral structure for both the cases. Both the complexes exhibited some non-covalent interactions, like π…π stacking, H-bonding contacts etc. **L**, **I** and **II** had also been found to possess fluorescence property. Anticancer activities of **L**, **I** and **II** had been investigated and it was found that both the complexes **I** and **II** were stronger cytotoxic agents against the breast cancer cell line MCF7 than the primary ligand system; while all of them (**L**, **I** and **II**) were less toxic against a non-cancerous cell line HEK293. All the compounds had shown potential photocatalytic activity in degrading methylene-blue (MB).

Keywords Co^{II} and Ni^{II} complexes · Crystal structures · π…π stacking · Anticancer activity · Photocatalytic activity.

1 Introduction

One of the most fascinating five-membered heterocyclic compounds of azole group is pyrazole, the ring of which contains two nitrogen atoms and a doubly unsaturated bond, can function as a primary donor site and has drawn a lot of interest as a ligand in formation of coordination complexes [1-4]. In recent years, pyrazole-based Schiff base ligands have attracted a lot of attention in forming various coordination polymers with different metal ions [5-10]. Schiff bases are some of the most extensively exploited imine compounds because of their utilization as pigments and dyes, catalyst carriers, polymer stabilizers, corrosion inhibitors and thermostable substances in addition to having a broad range of biological activities such as antibacterial, antimicrobial, antimalarial, antituberculosis, anticancer, anti-inflammatory and antifungal properties [11-14]. The imine or azomethine (-CH=N) group is thought to be responsible for the diverse biological characteristics of Schiff bases [15-19].

Cancer is the major public health hazard and is the second foremost reason for death all over the world. Among them breast cancer is an extremely dangerous tumor that kills numerous women globally [20]. Possessing anticancer activity by inhibiting the growth / propagation of carcinoma cells is one of the most fascinating biological properties of Schiff bases and their metal ion complexes. Detection of the antitumor activity of Schiff bases and their complexes against various tumour cell lines attracts the scientists to develop new anticancer drugs without any or a very little side effects (21-23) Numerous coordination compounds of Schiff base ligands particularly with heterocyclic moieties and different metal ions have already been applied to diagnose different malignancies and other diseases and registered substantial improvement of the ailments [24-29].

On the other hand, it is a fact that presently dyes are one of the most applied materials and are being used in numerous industries like textile, paint, leather, printing, paper industries etc. However, a large number of dyes viz., methylene violet (MV), methylene blue (MB), methyl

orange (MO), rhodamine B (RhB), etc., get released / discharged directly along with industrial wastewater into the environment is considered to be the potential source of pollutants and one of the key reasons for water pollution that affects aquatic creatures and cause eutrophication [30, 31]. These dyes are nonbiodegradable molecules comprising of composite aromatic structures and might bring about numerous adverse effects like mutagenic, carcinogenic or allergic interactions on various human body parts like liver, pancreas, kidneys or nervous system [32-35]. Coordination complexes containing Schiff-base ligands have recently received a lot of attention in degrading various dye molecules photo-catalytically. Their outstanding catalytic photodegradation efficacy and inexpensive experimental setup have created much interest [30, 36, 37]. The technique of photocatalysis is relied on the generation of hydroxyl radicals ($OH^{\bullet}$), which may quickly and non-selectively oxidize typical organic dyes and degrade them [38, 39].

Here we have described the synthesis, spectroscopy and X-ray crystallography of two Co^{II} and Ni^{II} complexes, $[Co(MPAFA)_3].2Br.2H_2O$ (**I**) and $[Ni(MPAFA)_3].2Br.2H_2O$ (**II**), respectively, of the Schiff-base, MPAFA (**L**), having 'NN' donor sites. In both the complex species, the metal centres acquire a hexa-coordinate distorted octahedral geometry. All the compounds (**L**, **I** and **II**) are capable of showing fluorescence activity and strong anticancer properties against MCF7, a human breast cancer cell line. They have been found to be less toxic against a non-cancerous cell line HEK293. Degradation of the methylene blue (MB) dye by photocatalysis in presence of the compounds have also been reported here. All of them (particularly **I** and **II**) are found to be efficient photo catalysts.

2 Experimental

The Chemicals and the reagents used in this study were of analytical grade, and purchased from available local vendors, and used as such without any additional purification. Spectro-grade solvents were employed for the measurements of conductance and spectra of the compounds.

2.1 Synthesis of the complexes: $[Co(MPAFA)_3].2Br.2H_2O$ (I) $[Ni(MPAFA)_3].2Br.2H_2O$ (II)

The Co^{II} and Ni^{II} complexes had been synthesized by refluxing a 3:1 molar mixture of the primary ligand, MPAFA [40] (0.3968 gm, 0.0021 mol) and 0.0007 mol each of $CoBr_2.6H_2O$ (for **I**) and $NiBr_2.6H_2O$ (for **II**) salts in ethanol on a boiling water bath for 1 hour (Scheme 1). Evaporating the subsequent reddish (for **I**) / light green (for **II**) solutions slowly on air, the required Co^{II} / Ni^{II} complexes isolated out as pink / green microcrystalline solid, respectively (Yield~76-78%). Diffraction quality single crystals of **I** and **II** had been grown in dichloromethane-n hexane mixture following solvent-diffusion technique. Anal. Calcd. (%) for $C_{30}H_{37}Br_2N_9CoO_5$ (**I**): C, 43.8; H, 4.5; N, 15.3; Co, 7.1. Found (%): C, 43.3; H, 4.2; N, 15.0; Co, 7.09. Λ_m(MeOH): 98 $\Omega^{-1}cm^2mol^{-1}$ at 30^0C. IR (4000-450 cm^{-1}, KBr) ν(cm^{-1}): 1571 ($\nu_{C=Npz,}$), 1632 ($\nu_{CH=Nazom}$), 469 ($\nu_{Co-Nazom}$) and 1046 (ν_{N-Npz}). UV–Vis. (MeOH, $\lambda_{max,}$ nm): 278($n\rightarrow \pi^*$), 240($\pi\rightarrow \pi^*$), 580(d–d). μ_{eff} 1.78 BM at 300K.

Anal. Calcd. (%) for $C_{30}H_{37}Br_2N_9NiO_5$ (**II**): C, 43.9; H, 4.8; N, 15.4; Ni, 7.3. Found (%): C, 43.4; H, 4.3; N, 15.1; Ni, 7.1. Λ_m(MeOH): 185 $\Omega^{-1}cm^2mol^{-1}$ at 30^0C. IR (4000-450 cm^{-1}, KBr) ν(cm^{-1}): 1578 ($\nu_{C=N,\ pyrazole}$), 1633 ($\nu_{CH=N,\ azomethine}$), 481 ($\nu_{Ni-N,\ azomethine}$) and 1075 ($\nu_{N-N,\ pyrazole}$). UV–Vis. (MeOH, $\lambda_{max,}$ nm): 213($\pi\rightarrow \pi^*$), 249($n\rightarrow \pi^*$), 569(d–d). μ_{eff} 2.89 BM at 300K.

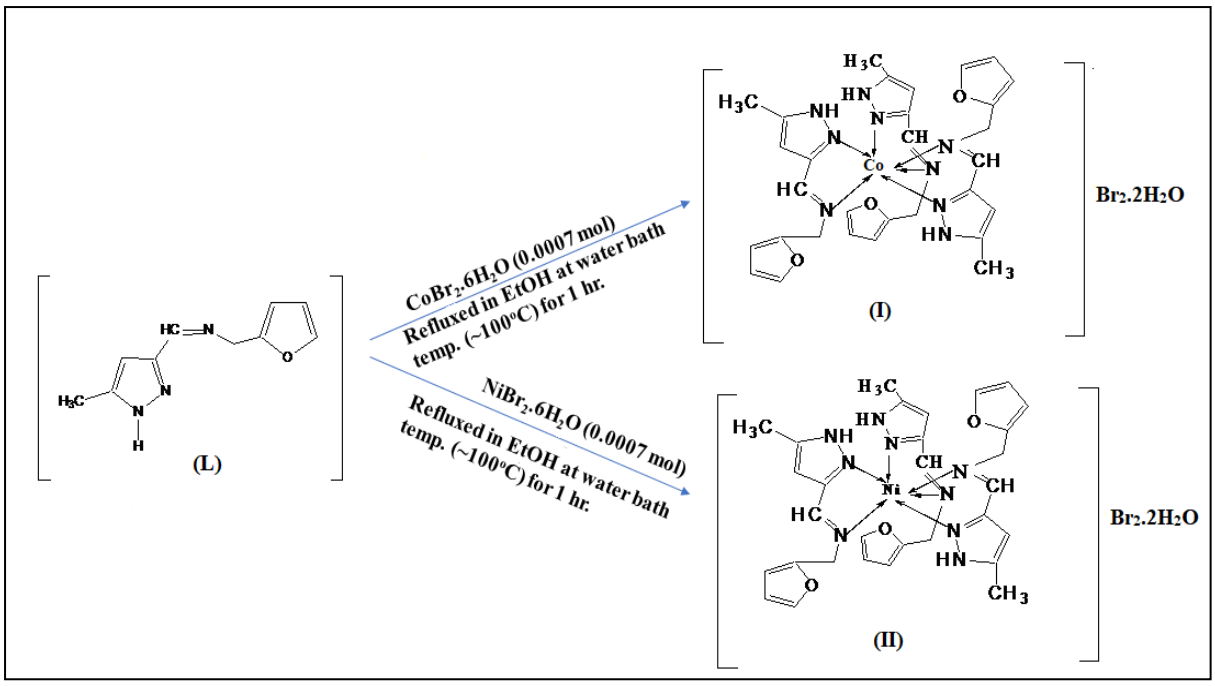

Scheme 1 Synthetic pathway of the complexes

2.2 Physical measurements

A Systronics 306 digital conductivity metre was used to measure the molar conductance of the complexes in methanol solutions. The elemental analyses (C, H, and N) were performed using a Perkin-Elmer 2400 CHNS/O analyser. The amount of Co and Ni present in the complexes had been estimated gravimetrically as anhydrous $CoSO_4$ and dimethylglyoximatonickel(II), respectively. A PAR 155 sample vibrating magnetometer was employed to evaluate the magnetic susceptibilities of the complexes in polycrystalline form. A Perkin Elmer Model Spectrum Two FT-IR spectrophotometer was used to record the IR spectra (4000-450 cm^{-1}) of the complexes using KBr pellets. Solution spectra of complexes in MeOH were recorded on a Shimadzu UV-1900i spectrophotometer. The fluorescence spectra of the complexes in MeOH were measured using a Hitachi F-7100 Fluorescence Spectrometer. Photodegradation of methylene blue (MB) had been investigated using a Shimadzu UV-1900i spectrophotometer. During the irradiation process, a UV-400 type photochemical reactor equipped with a 400W mercury lamp served as the UV and visible light source.

2.3 Single crystal X-ray structure determination

The Rigaku MM-007HF High Brilliance RA generator/confocal optics with XtaLAB P100 diffractometer [Cu Kα radiation (λ =1.54187 Å)] was used to acquire the X-ray diffraction data for **I**. A Rigaku FR-X Ultrahigh Brilliance Microfocus RA generator/confocal optics with XtaLAB P200 diffractometer [Mo Kα radiation (λ = 0.71073 Å)] was used to collect the data for **II** at 173 K. ω steps were used to collect all intensity data. Area detector images spanning at least a hemisphere of reciprocal space were accumulating. The data had been collected using CrystalClear [41] and analysed using CrysAlisPro [42] (including correction for Lorentz, polarisation, and absorption). Direct methods (SIR2004 [43]) was used to solve the structures and full-matrix least-squares against F^2 (SHELXL-2018/3 [44]) was employed to refine the structures. Anisotropic refinement was applied to non-hydrogen atoms, while a riding model was used to refine carbon-bound hydrogen atoms. The difference Fourier map was utilized to locate the heteroatom-bound hydrogen atoms, which were then refined isotropically while being constrained by distance. The CrystalStructure [45] interface had been used to perform all calculations.

2.4 Anticancer activities of the compounds

2.4.1 Cell culture

In this study, both the hormone-responsive breast cancer cell line MCF7 and non-cancerous human embryonic cell line HEK293 were used, kept at 37 °C in an incubator with humidified 5% CO_2 and DMEM (Gibco) [46] supplemented with 10% foetal bovine serum and penicillin-streptomycin. The cells were not subjected to any additional studies until they had reached 70% confluence.

2.4.2 Viability testing of cells

MTT assay was employed to determine the viability of cells against various dosages of synthesized compounds **L**, **I** and **II**. Seeding of cells was done at a density of 3×10^3 cells/well in a 96-well plate and were treated with progressively increasing concentrations of **L**, **I** and **II**.

Upon expiry of 24 hours of experiment, MTT and PBS were added to the wells and allowed to keep at 37˚C for 3 hours. After that removal of the media containing MTT and PBS was made, followed by the addition of 100 µl of DMSO to make the formazan crystals [47], indicators of mitochondrial function, soluble. In the Bio Rad iMark^{TM} Microplate Reader, absorbance was measured at 590 nm. The IC_{50} concentrations for each compound were calculated using linear trendline equation.

2.4.3 Detection of Reactive Oxygen Species Generation

The level of generation of reactive oxygen species (ROS) within the cells was evaluated by DCFDA assay. Following the treatment of cells with the synthesized compounds, H_2DCFDA was added to phenol-red-free DMEM, the treated cells were incubated in the same for 45 minutes [48]. After the incubation period was over, cells were thoroughly washed with 1X PBS before being examined under a 40X fluorescent microscope.

2.5 Photocatalytic experiment

Using methylene blue (MB) as the target dye, the photocatalytic activity of the compounds **L**, **I**, and **II** was investigated. The steps of the experiment were as follows: Prior to the photocatalytic degradation experiment, each compound under investigation should be well dispersed in dye solution. 100 mL of MB aqueous solution (10 mg/L) must contain 0.02 mmol of each solid compound. Before being exposed to ultraviolet radiation, the resultant solutions of the compounds were magnetically stirred for an hour in dark till an equilibrium of adsorption-desorption attained. The mixture was then exposed to UV and visible light for the following 105 mins, samples were being collected every 15 mins interval throughout this time, and their absorbance was continually measured. To determine the photosensitivity of MB, the blank experiment (without the addition of catalysts) was performed under the same

experimental condition. The following formula was utilized to calculate the degradation efficiencies of the photocatalysts: $D\% = A_t/A_0 x100\%$

Where A_0 represents the initial absorbance values of the MB aqueous solution; D% represents photocatalyst degradation efficiencies; and A_t represents the absorbance values of the MB aqueous solution at time t.

3 Results and discussion

3.1 Structural Description

The molecular views of the complexes, **I** and **II** together with the π…π stacking and potential H-bonding interactions were shown in Figs. 1 and 2, respectively. Table 1 provided an overview of the crystallographic data and refinement parameters. Both the monomeric complexes **I** and **II** crystallized in the monoclinic space group *P2₁/c*. A $[M(MPAFA)_3]^{2+}$cation (M = Co/Ni), two Br^- as counter anions and two molecules of water as solvent of crystallization made up the asymmetric units in the structures of both **I** and **II**. Some of the relevant bond distances and angles observed in the complexes were depicted in Table 2. Both **I** and **II** were found to be six coordinate distorted octahedral species containing CoN6 and NiN6 donor sets about the Co^{II} and Ni^{II} centres, respectively. **L** behaved as a bidentate ligand and formed M:L::1:3 complexes in both the cases. Each molecule of **L** had been found to coordinate to the metal ion via the pyrazolyl (tertiary) ring nitrogen atoms [N2, N16 and N30] and the azomethine nitrogen atoms [N7, N21 and N35]. Due to such coordination, three stable 5-membered chelates, such as [M-N30-C31-C34-N35], [M-N16-C17-C20-N21] and [M-N2-C3-C6-N7], (where M = Co, Ni) were generated. <N2-Co1-N7=76.75(7)°, <N16-Co1-N21=76.66(8)° and <N30-Co1-N35=77.85(8)° were the bite angles of the chelates formed in **I**; the similar angles for **II** were found to be <N2-Ni1-N7=78.65(16)°, <N16-Ni1-N21=77.89(16)° and <N30-Ni1-N35=77.77(15)°. In both the complex species, a meridional

coordination mode was shown by the pyrazolyl ring nitrogen atoms and the azomethine nitrogen atoms. The azomethine groups present in the complex molecules needed to be planar due to the formation of the chelate ring and the possibility of conjugation, whereas the methyl-furan groups were not present in the same planes but rather existed in a pendant fashion, making them almost orthogonal to the planes of the other ligands [40].

In **I**, two bromide counter ions (Br1 and Br2) and one molecule of water of crystallization (O51) were held by extensive hydrogen bonding interactions, viz., N15–H15…Br1, N1–H1…O51, O51–H51B…Br2, etc. (Fig. 1). Likewise, in **II** also, two bromide counter ions (Br1 and Br2) and two molecules of water of crystallization (O51& O52) were detained by extensive hydrogen bonding interactions, viz., N15–H15…Br1, N29–H29…O51, O52–H52A…Br2, etc. (Fig. 2). The H-bonding interactions seen in **I** and **II** were depicted in Tables S1 and S2, respectively. In addition to H-bonding, both **I** and **II** had also possessed substantial intramolecular $\pi\ldots\pi$ stacking interactions between the furan ring of one ligand and the pyrazole ring of another ligand; the centroids of the furan and pyrazole rings were separated by a distance of 3.850 Å for **I** and 3.831 Å for **II** (Figs. 1 and 2). The both **I** and **II**, the observed stacking interactions were found to be moderately strong [49,50] and made the complex molecules more stable. The packing diagrams of **I** and **II** were represented in Figs. S1 and S2, respectively.

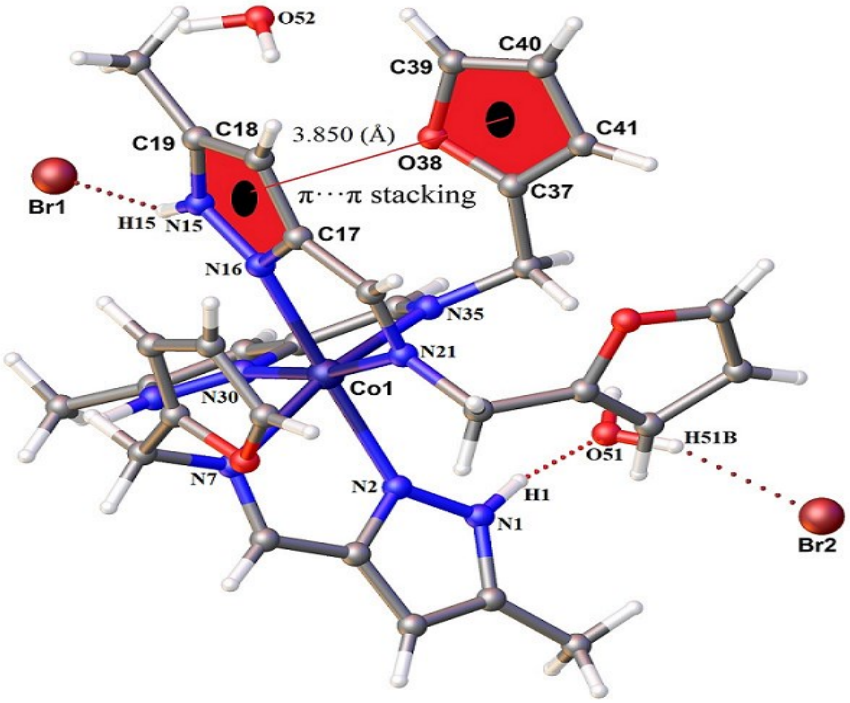

Fig. 1 View of the molecular structure of **I** showing few of the potential hydrogen bonding and π…π stacking interactions observed in the molecule.

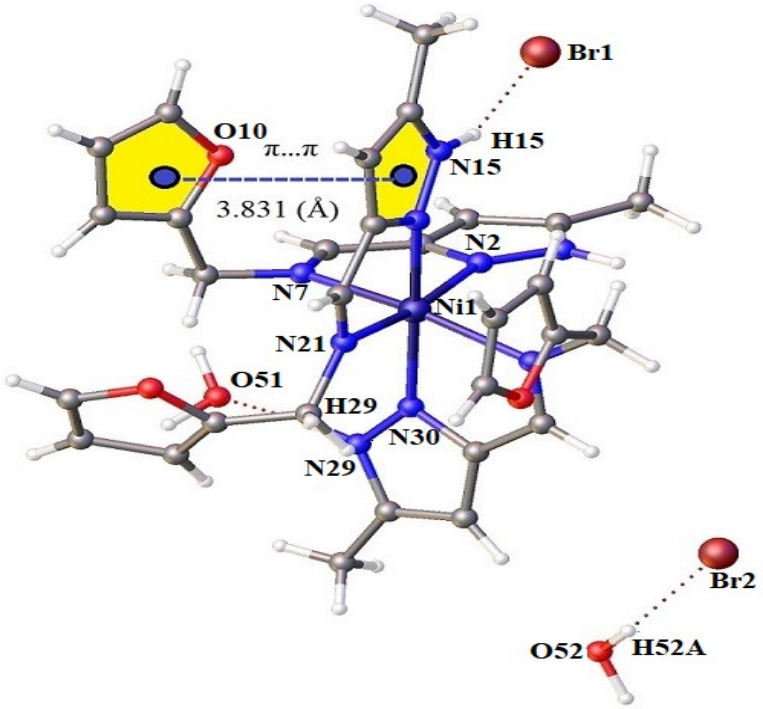

Fig. 2 View of the molecular structure of **II** showing few of the potential hydrogen bonding and π…π stacking interactions observed in the molecule.

Table1 Crystal data and structure refinement parameters for complexes **I** and **II**

Crystal data	**[Co(MPAFA)$_3$].2Br.2H$_2$O (I)**	**[Ni(MPAFA)$_3$].2Br. 2H$_2$O (II)**
Emp. Formula	$C_{30}H_{37}Br_2CoN_9O_5$	$C_{30}H_{37}Br_2N_9NiO_5$
F. wt.	822.43	822.19
Temp/K	173	173
Crystal system	monoclinic	monoclinic
Space group	$P2_1/c$	$P2_1/c$
a/Å α/°	10.36740(10) 90	10.3745(3) 90.000
b/Å β/°	16.7987(2) 97.9990(10)	16.7936(5) 97.820(3)
c/Å γ/°	20.1822(2) 90	20.0949(6) 90.0000
Vol/Å^3	3480.71(6)	3468.48(18)
Z	4	4
ρ_{calc}g/cm^3	1.569	1.574
μ/mm^{-1}	6.987	2.922
F(000)	1668.0	1672.0
Crystal size/mm^3	0.2 × 0.09 × 0.06	0.150 × 0.070 × 0.020
Radiation	CuKα (λ = 1.54184)	Mo Kα (λ = 0.71073)
2Θ range for data collection/°	6.874 to 136.78	3.172 to 58.072
Index ranges	-12 ≤ h ≤ 12, -20 ≤ k ≤ 20, -21 ≤ l ≤ 24	-14 ≤ h ≤ 13, -22 ≤ k ≤ 22, -25 ≤ l 25
Reflections collected	36373	43776
Independent reflections	6335 [R_{int} = 0.0278, R_{sigma} = 0.0192]	7991 [R_{int} = 0.0462, R_{sigma} =0.033
Data/restraints/parameters	6335/7/455	7991/11/451
Goodness-of-fit on F^2	1.066	1.071
Final R indexes [I>=2σ (I)]	R_1 = 0.0304, wR_2 = 0.0835	R_1 = 0.0865, wR_2 = 0.2080
Final R indexes [all data]	R_1 = 0.0318, wR_2 = 0.0844	R_1 =0.1096, wR_2 =0.2260
Largest diff. peak/hole/ e Å^{-3}	0.64/-0.94	1.75/-0.38

Table 2 Some of the relevant bond lengths (Å) and angles (°) of $C_{30}H_{37}Br_2N_9CoO_5$ (**I**) and $C_{30}H_{37}Br_2N_9NiO_5$ (**II**)

Bond lengths(Å)	**I**	Bond lengths (Å)	**II**
Co1-N2	2.1012(19)	Ni1-N2	2.079(4)
Co1-N7	2.175(2)	Ni1-N7	2.129(4)
Co1-N21	2.170(2)	Ni1-N21	2.122(4)
Co1-N16	2.0758(19)	Ni1-N16	2.036(4)
Co1-N30	2.1062(19)	Ni1-N30	2.073(4)
Co1-N35	2.1615(19)	Ni1-N35	2.134(4)
Bond Angles (º)		Bond Angles (º)	
N2 -Co1- N7	76.75(7)	N2- Ni1-N7	78.65(16)
N7 -Co1- N21	86.60(7)	N7- Ni1-N21	98.69(15)
N21 -Co1- N16	76.66(8)	N21- Ni1-N16	77.89(16)
N16 -Co1 -N35	92.60(8)	N16- Ni1-N35	99.24(16)
N35 -Co1 -N2	90.84(7)	N35- Ni1-N2	96.25(15)
N30 -Co1 -N7	97.45(7)	N30- Ni1-N7	91.01(15)
N30 -Co1 -N35	77.85(8)	N30- Ni1-N35	77.77(15)
N30 -Co1 -N21	170.39(7)	N30- Ni1-N21	96.28(16)
N2 -Co1 -N21	96.98(7)	N2- Ni1-N21	171.56(16)
N16 -Co1 -N30	94.00(8)	N16- Ni1-N30	173.61(16)
N35 -Co1 -N7	166.62(8)	N35- Ni1-N7	167.60(15)
N2 -Co1 -N16	173.21(8)	N2- Ni1-N16	94.15(15)
N16 -Co1 -N7	100.27(8)	N16- Ni1-N7	92.44(16)
N35 -Co1 -N21	100.04(7)	N35- Ni1-N21	87.90(15)
N30 -Co1 -N2	92.45(7)	N30- Ni1-N2	91.79(15)

3.2 Spectroscopic characterization of the complexes

The unique infrared bands (4000-450 cm^{-1}, KBr) of the un-complexed **L**, when compared to those of **I** and **II** provided valuable information on the binding sites of **L** molecule. A red shift of 1632-1633 cm^{-1} in the complexes in compared to the $\nu_{(CH=N,\ azomethine)}$ (1650 cm^{-1}) band in the spectrum of **L** was consistent with the coordination of the central metal ion with the azomethine nitrogen. A blue shift of 1571-1578 cm^{-1} in the complexes in compared to the $\nu_{C=N(pyrazole\ ring)}$ (1540 cm^{-1}) band observed in the free ligand spectrum was indicative of the pyrazole ring nitrogen atom (^{2}N) as a plausible binding site. A reasonably strong band appeared

at 1010 cm^{-1} in the spectrum of **L** due to the $\nu_{N\text{-}N(pyrazole)}$ vibration, was also suffered blue shifts of 1046-1075 cm^{-1} in the complexes. This provided further indication that the tertiary nitrogen (^2N) atom in the pyrazole ring participated in bonding [51, 52]. The new bands found at 469-481 cm^{-1} in the spectra of **I** and **II**, might be assignable to $\nu_{(M\text{-}N,\ azomethine)}$ bonds [40,51,52]. The absorption spectra of **I** and **II** in methanol, the ligand to metal charge transfer (LMCT) bands were found visible at 213–240 ($\pi \rightarrow \pi^*$) and 249-278 ($n \rightarrow \pi^*$) nm, respectively, as well as a low intensity broad band due to the d–d transition of metal ion at 580–569 nm was also registered [53].

3.3 Luminescence property

The room temperature fluorescence spectra of all the compounds (**L**, **I** and **II)** were recorded in methanol solution at $2x10^{-5}$ M concentration. All of them were found to exhibit characteristic fluorescence properties. The emission bands were visible between 460-440 nm when the compounds got excited at wavelengths between 249-236 nm (Fig.3, Table S3). Among the three compounds, **L** was found to possess more fluorescent activity. At the excitation wave length of 236 nm, it showed a strong emission band at the maximum emission wavelength of 440 nm. No detectable emission was noticed when the excitation wavelength altered. According to the observations, compound **L** was more luminescent than the complexes **I** and **II**. During complex formation by a transition metal ion, fluorescence quenching of the ligand was a normal incidence. Various interactions / factors such as excited-state reactions, ground-state complex formation, perturbation of magnetic field, redox phenomena, presence of heavy metal etc. can explain the quenching phenomena [54-57].

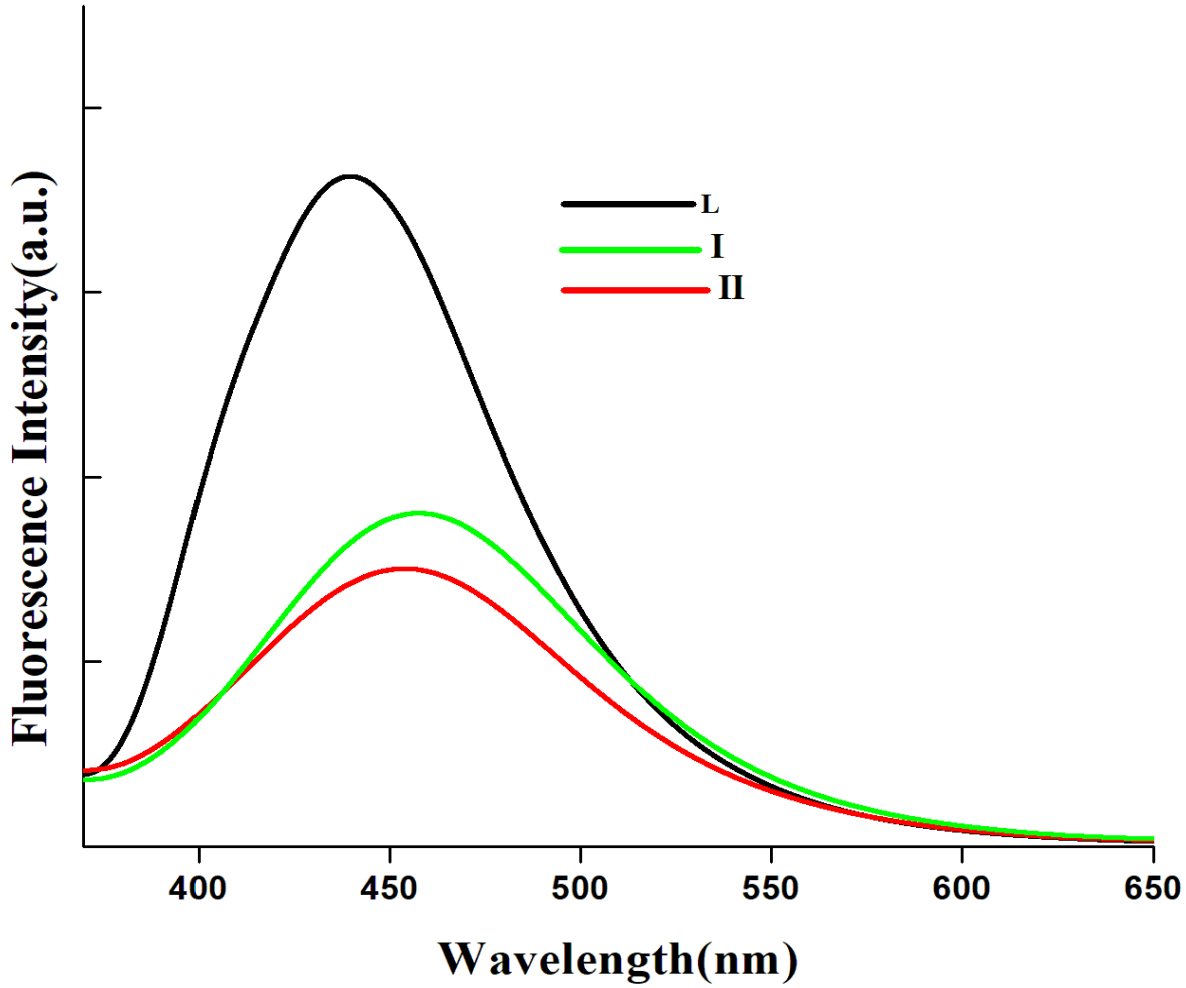

Fig. 3 Fluorescence spectra of the ligand and the complexes in MeOH; [MPAFA] (**L**), $[Co(MPAFA)_3].2Br.2H_2O$ (**I**) and $[Ni(MPAFA)_3].2Br.2H_2O$ (**II**)

3.4 Anticancer activities of the compounds

3.4.1 In vitro cytotoxic effect of the compounds **L, I** and **II** on **MCF7** and **HEK293**

To determine whether the compounds exerted any cytotoxic effect on HEK293 cells and MCF7 cells, MTT assay had been executed, by treating the cells with progressively increasing concentrations (at a range of 1 µM to 100 µM) of **L**, **I** and **II** for 24 hours. IC_{50} values were calculated from the linear trendline equations prepared by plotting doses against the respective % of cell viability along the X and Y axes, respectively (Figs. 4 and S3, Table 3). The findings

unequivocally demonstrated that both **I** and **II** were stronger cytotoxic agents than **L**, which was indicative of the fact that added functional groups / metal ions considerably increased the cytotoxic activity. Moreover, significantly high selectivity indices of these compounds reflected that these compounds can be used as potent anti-cancer agents. **I** exerted the highest selectivity index of 1.88 indicating its potential to be a therapeutic agent as selectivity indices between 1.5-2.0 or greater than 2 are considered to be indicators of drug ability.

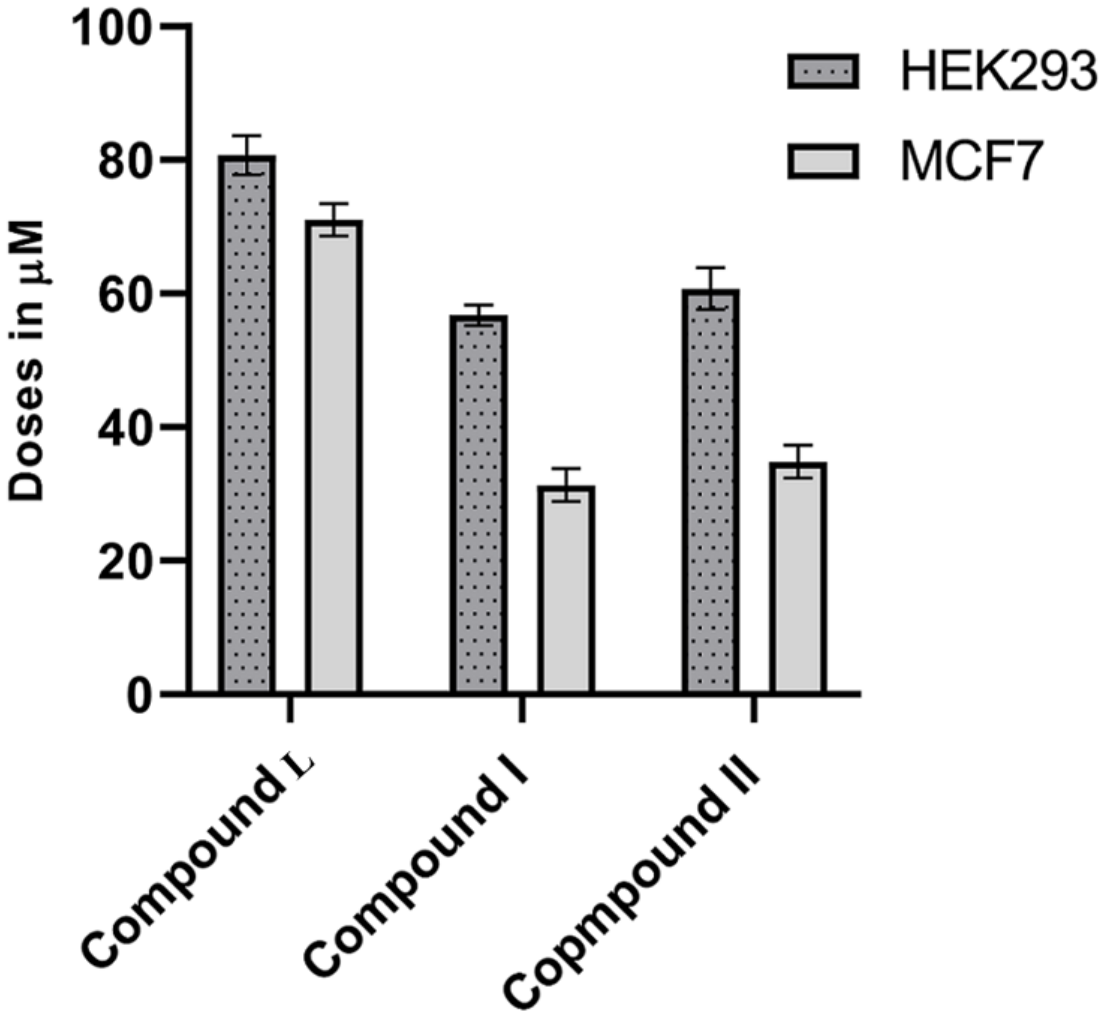

Fig. 4 IC_{50} values of **L**, **I** and **II** on HEK293 cells and human breast cancer cell line MCF7 upon 24 hours of treatment

Table3 IC50 values of **L**, **I** and **II** on HEK293 and MCF7 cell line

Compounds	IC50 at 24 hours (µM) on HEK293	IC50 at 24 hours (µM) on MCF7	Selectivity Index
L	82.799 ± 3.45	72.736 ± 2.51	1.14
I	55.672 ± 2.74	29.56 ± 0.77	1.88
II	58.546 ± 2.89	33.09 ± 0.98	1.76

3.4.2 The compounds (L I and II) were proficient of generating Reactive Oxygen Species (ROS) in MCF7 cell line

The substantial cytotoxic property of the compounds sparked intense interest in understanding how these compounds cause cytotoxicity. We used the DCFDA assay to determine whether these substances are releasing reactive oxygen species into the cells and thereby causing cytotoxicity. The fluorescence microscopy images clearly reflected that compared to untreated cells; the fluorescence intensity dramatically increased after the compounds were added to the cells. This observation also showed that after 24 hours of exposure to the ligand and the complexes, the quantity of ROS increased significantly (Fig.5) on treating MCF7 with the complexes.

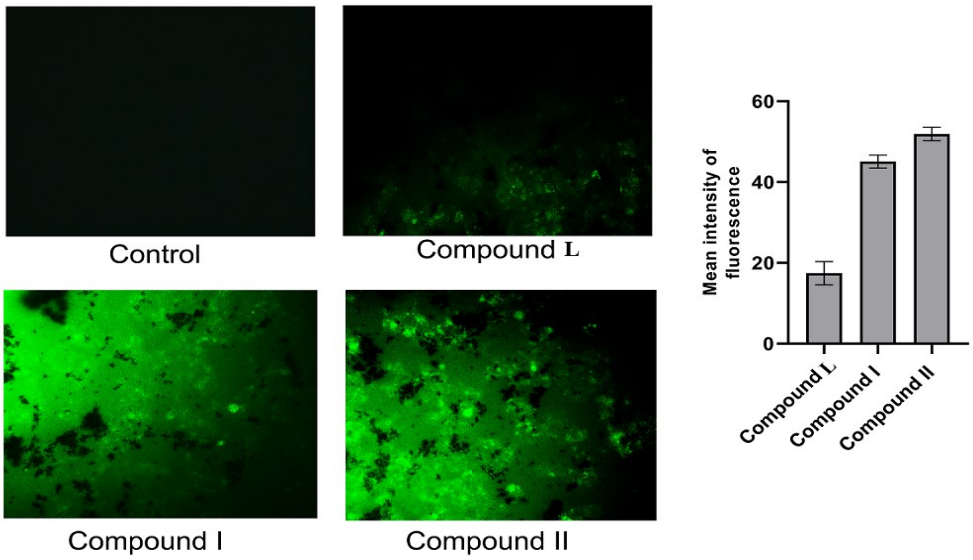

Fig. 5 Fluorescence microscopy images of treated and untreated MCF7 cells acquired from DCFDA assay and bar diagrammatic depiction of the fluorescence intensity conforming to the level of ROS generation upon 24 hours of treatment with **L**, **I** and **II**

3.5 Photocatalytic study

The elimination of organic pollutants from water using green photocatalysts is a well-known application for several Schiff base complexes [58]. On promotion of an electron from the HOMO to the LUMO, UV-Vis radiation causes organic ligands to generate O and/or N-metal charge transfer during the photocatalytic process. An electron must come back to the steady state of the HOMO in order for it to function. The photocatalytic process was thus completed by capturing one electron from oxygenated water molecules, resulting in the $OH^{\bullet}$ active species [59]. Methylene blue (MB), the most widely used organic dye, was chosen as the model pollutant to assess the photocatalytic efficiency of the compounds (**L**, **I** and **II**) in aqueous media. First, a blank experiment (Only UV light, no MB) was used to assess the stability of each compound. According to the UV-Vis (Fig. S4) and FTIR (Fig. S5) spectroscopy studies, there was no degradation of the compounds after 105 minutes of excessive radiation. Under the same conditions, the photo-degradation processes of MB alone (without adding compounds) had also been investigated for comparison. The photocatalytic behaviors of the ligand and its Co(II) and Ni(II) complexes in MB solution were shown in Figs. 6, 7 and 8, respectively. As the irradiation time was increased, the typical MB aqueous solution absorption peaks became progressively weaker. The degradation efficiencies of MB by photocatalysis were increased in the presence of compounds **L**, **I** and **II**, reaching up 66.7% for **L**, 91.3% for **I**, 93.8% for **II** after 105 min of UV irradiation, severally, (Fig. 9). The degradation efficiency of the control experiment was just 16.8% (k_4=0.00149 min^{-1}) in 105 minutes, demonstrating that the MB solution without catalyst had weak self-photosensitivity (Fig. 9). It was clear that

compounds **L**, **I** and **II** exhibited strong photocatalytic activity for the breakdown of MB. These findings confirmed that MB degradation requires the presence of catalysts. The ligand (**L**) in this instance was less active than the corresponding metal complexes (**I** and **II**). In fact, the degradation efficiency of MB after 105 min was 66.7% for the free ligand. These experimental results implied that effectiveness of photodegradation of MB might be significantly influenced by the type of metal ion that is present in the complexes [60]. The following equation described how the photocatalytic degradation of MB in aqueous solution was determined using the pseudo-first-order kinetic equation:

$-\ln(A/A_0) = kt$ .....(1)

When $-\ln(A/A_0)$ was plotted against t (A=maximum absorbance of MB at variable irradiation time 't', A_0=maximum absorbance of MB at initial time of irradiation), three straight lines passing from the origin with slopes of 0.01165 (K_1=0.01165 min^{-1}), 0.01454 (K_2=0.01454min^{-1}) and 0.01812 (K_3=0.01812 min^{-1}), for **L**, **I** and **II**, respectively, were obtained (Fig. 10). According to this result, **I** and **II** had degradation efficiencies of more than 90% when behaved as UV-response photocatalysts to degrade the Organic dye pollutants. The degradation efficiency of the compounds was closely matched with data published earlier [38,39,61,62].

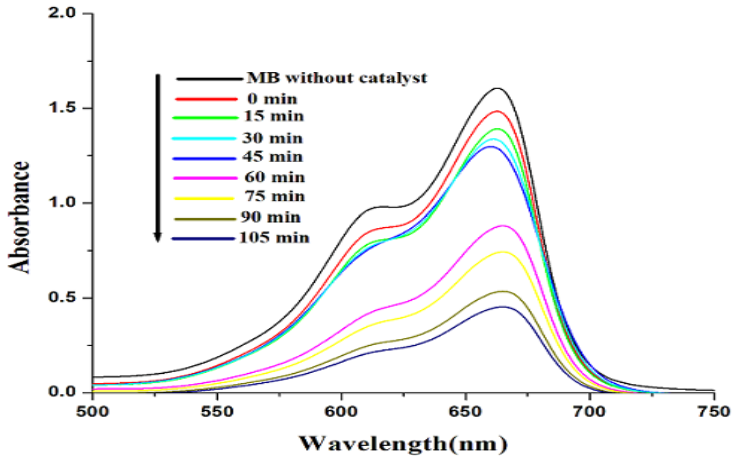

Fig.6 The absorption spectra of the MB solutions during the degradation reaction under UV light irradiation in the presence of **L**

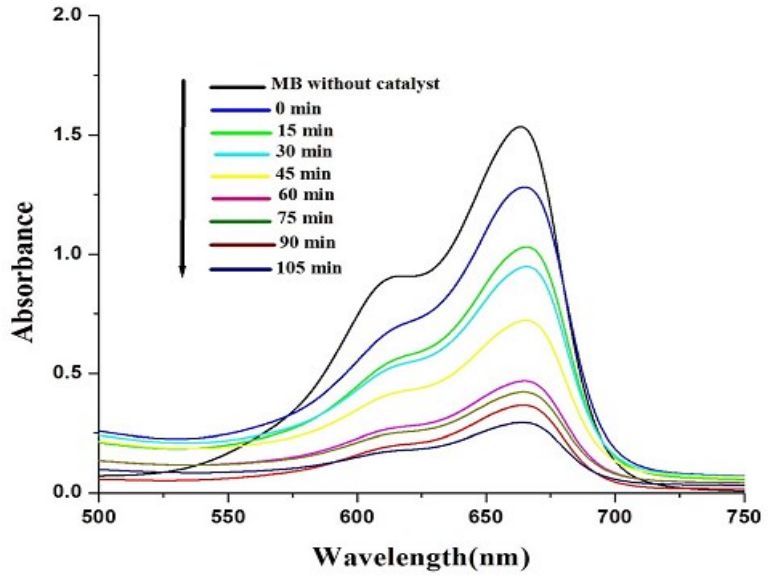

Fig.7 The absorption spectra of the MB solutions during the degradation reaction under UV light irradiation in the presence of **I**

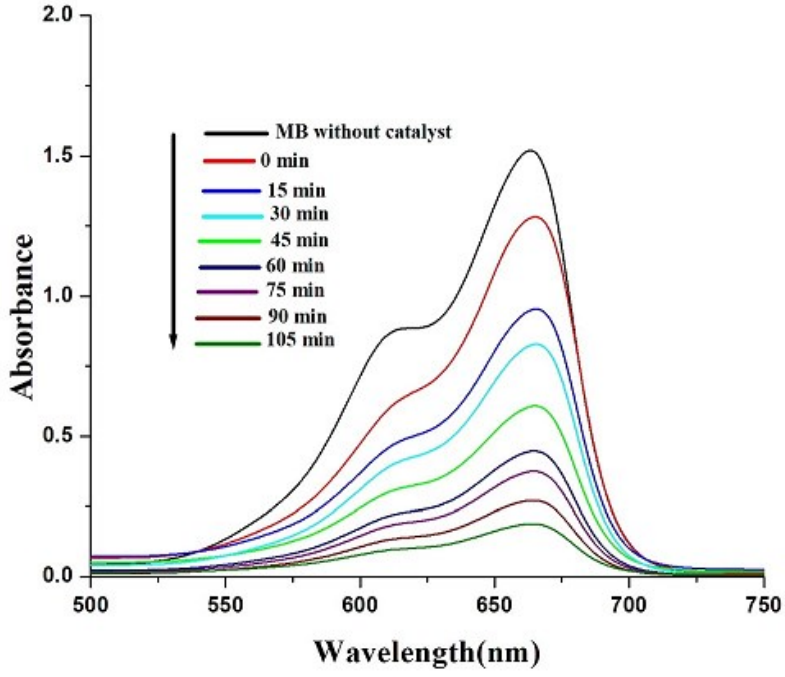

Fig. 8 The absorption spectra of the MB solutions during the degradation reaction under UV light irradiation in the presence of **II**

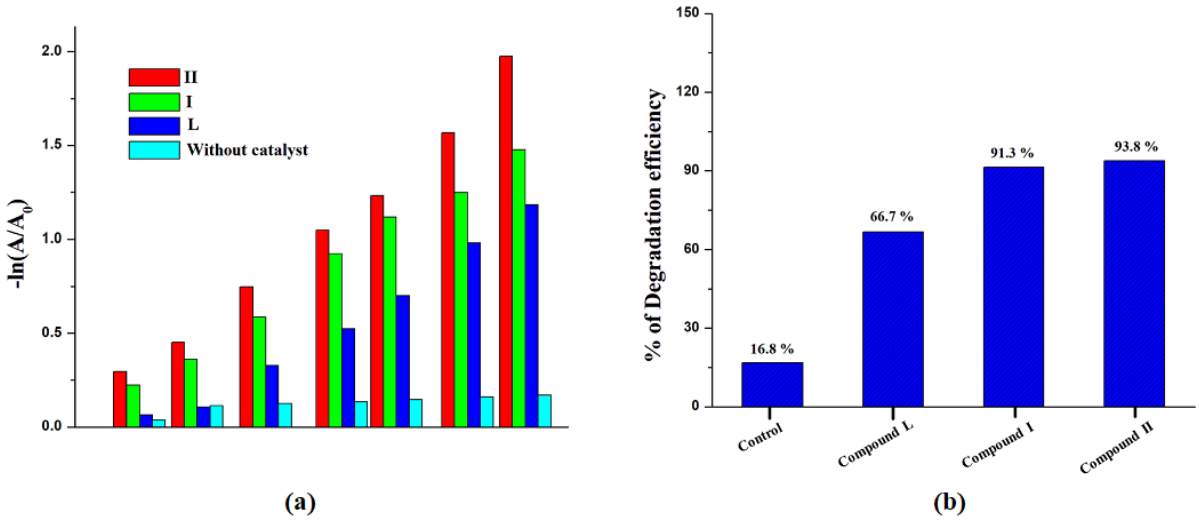

Fig. 9 (a) Bar diagrammatic representation of the pseudo-first-order plot of MB solution upon 105 minutes of UV light irradiation with the use of **L, I** & **II**; **(b)** Percent of MB dye degradation efficiency of the catalyst **L, I** and **II** upon 105minutes of UV light irradiation

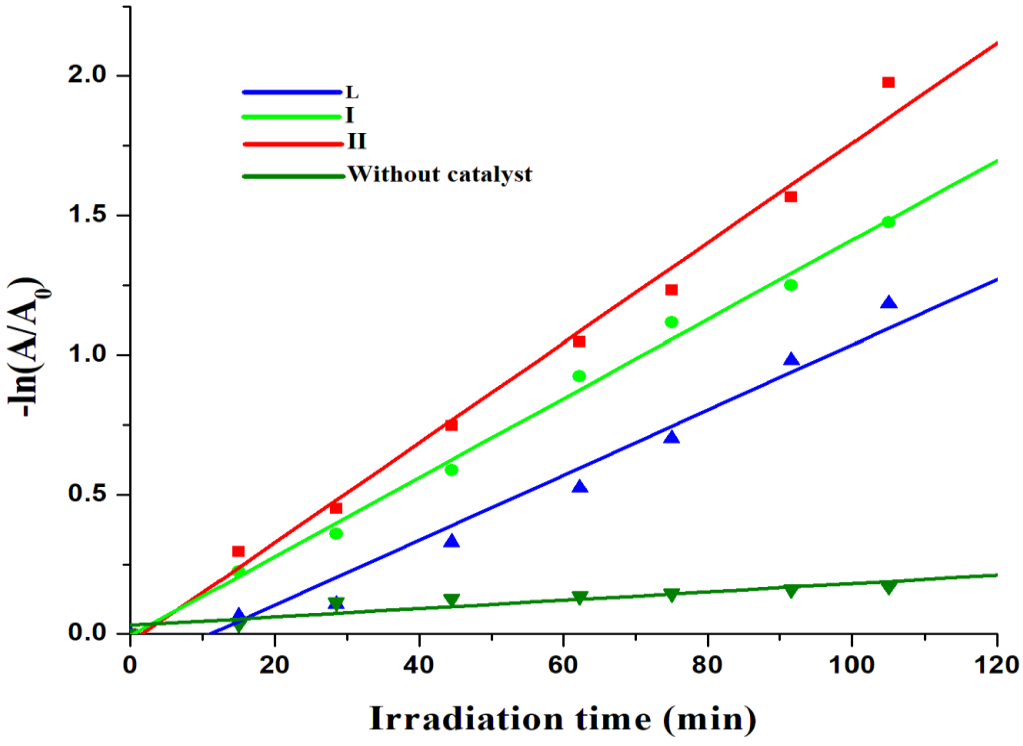

Fig. 10 The pseudo-first-order plot of MB solution under UV light irradiation with the use of **L, I** and **II** and no crystal in the same conditions (**L**: K_1=0.01165 min^{-1}, **I**: K_2=0.01812 min^{-1}, **II**: K_3=0.01454 min^{-1}, without catalyst**:** K_4=0.00149 min^{-1}).

4 Conclusions

The present communication was engaged in reporting the synthesis, characterisation, X-ray crystallography, photocatalytic and anticancer activities of the Co^{II} and Ni^{II} complexes of the potentially 'NN' bidentate ligand, MPAFA. The ligand had been found to react with Co^{II} and Ni^{II} ions in 1:3 (M:L) molar ratio to form distorted octahedral complexes comprising of CoN6 and NiN6 chromospheres, respectively. In both **I** and **II**, the bonding occurred through the pyrazole ring (tertiary) N atom and the azomethine N atom. All the compounds had been found to exhibit fluorescence property and **L** had been found more luminescent than **I** and **II**. The compounds had been screened for their anticancer property and it had been found that **I** and **II** were far more powerful cytotoxic agents than **L** itself against the breast cancer cell line MCF7, while all three were less toxic against HEK293, a non-cancerous cell line. The cytotoxic effects of the ligand and the complexes were believed to be caused by the increased generation of ROS, which might had brought about the cell death processes such as damage of DNA, peroxidation of lipid, apoptosis, and necrosis. The compounds (**L**, **I** and **II**) had demonstrated their abilities for photocatalytic degradation of MB dye and the complexes (**I** and **II**) were found more efficient in this field than the ligand **L**.

Statements and Declarations

Informed Consent Statement Not applicable.

Ethical approval Statement Not applicable.

Conflicts of interest No conflicts of interest are disclosed by the corresponding author on behalf of the other authors.

Supplementary Material

CCDC deposition numbers 1402319 and 2241317 contain the supplementary crystallographic data for the complexes **I** and **II**, respectively. These data can be obtained free of charge via http://www.ccdc.cam.ac.uk/conts/retrieving.html, or from the Cambridge Crystallographic Data Centre, 12 Union Road, Cambridge CB2 1EZ, UK; fax: (+44) 1223-336-033; or e-mail: deposit@ccdc.cam.ac.uk. Figures S1-S5 and Tables S1-S3 are available as supplementary materials.

References

1. Behr LC, Fusco R, Jarboe CH (1967) The Chemistry of Heterocyclic Compounds: Pyrazoles, Pyrazolines, Pyrazolidines, Indazoles and Condensed rings. Wiley & Sons, London

2. Ozkınalı S, Gur M, Sener N, Alkın S, Cavus MS (2018) Synthesis of new azo Schiff bases of pyrazole derivatives and their spectroscopic and theoretical investigations. J Mol Struct 1174:74-83. https://doi.org/10.1016/j.molstruc.2018.06.070

3. Ribeiro N, Roy S, Butenko N, Cavaco I, Pinheiro T, Alho I, Marques F, Avecilla F, Pessoa JC, Correia I (2017) New Cu(II) complexes with pyrazolyl derived Schiff base ligands: Synthesis and biological evaluation. J Inorg Biochem 174:63-75 https://doi.org/10.1016/j.jinorgbio.2017.05.011

4. Mandal S, Saha R, Saha M, Pradhan R, Butcher RJ, Saha NC (2016) Synthesis, crystal structure, spectral characterization and photoluminescence property of three Cd(II) complexes with a pyrazole-based Schiff-base ligand. J Mol Struct 1110:11-18 https://doi.org/10.1016/j.molstruc.2016.01.020

5. Sengupta S, Ganguly S, Goswami A, Bala S, Bhattacharya S, Mondal R (2012) Construction of Co(II) coordination polymers comprising of helical units using a flexible pyrazole based ligand. CrystEngComm 14:7428-7437. https://doi.org/10.1039/C2CE25256B

6. Torres-García P, Pedrero-Marín R, Luna-Giles F, Huertas-Sanchez AV, Vinuelas-Zahínos E (2012) Influence of steric strain of S, N-heterocycles derivative ligands on the coordination geometry in cadmium(II) nitrato complexes. Polyhedron 31:307-318. https://doi.org/10.1016/j.poly.2011.09.033

7. Konar S, Jana A, Das K, Ray S, Chatterjee S, Kar SK (2012) Complexes of a functionally modified pyrazole derived ligand – Mononuclear zinc(II), dinuclear nickel(II) and a rare pentanuclear cadmium(II) complex with a TBP core and their photoluminescence studies. Polyhedron 47:143-150.https://doi.org/10.1016/j.poly.2012.07.080

8. WangL, You W, Huang W (2009) Alteration of Molecular Conformations, Coordination Modes, and Architectures for a Novel 3,8-Diimidazol-1,10-phenanthroline Compound in the Construction of Cadmium(II) and Zinc(II) Homochiral Coordination Polymers Involving an Auxiliary Chiral Camphorate Ligand. Inorg Chem 48:4295–4305. https://doi.org/10.1021/ic802445q

9. Notash B, Safari N, Abedi A, Amani V, Khavasi HR (2009) Cadmium(II) complexes containing 2,2′-dimethyl-4,4′-bithiazole ligand: synthesis, characterization, and crystal structure. J Coord Chem 62:1638-1649. https://doi.org/10.1080/00958970802672978

10. Wang J, Yang S, Zhou A, Liu Z, Zhao J (2013) Two- and three-dimensional photoluminescent Cd(II)-carboxylate coordination frameworks bridged by benzenepentacarboxylate and N-donor ligands. J Coord Chem 66:2413-2422. https://doi.org/10.1080/00958972.2013.805410

11. Rocha M, Di Santo A, Echeverría GA, Piro OE, Cukiernik FD, Ulic SE, Gil DM (2017) Supramolecular self-assembly of a new multi-conformational Schiff base through hydrogen bonds: Crystal structure, spectroscopic and theoretical investigation. J Mol Struct 1133**:**24-36. https://doi.org/10.1016/j.molstruc.2016.11.071

12. Purtas F, Sayin K, Ceyhan G, Kose M, Kurtoglu M (2017) New fluorescent azo-Schiff base Cu(II) and Zn(II) metal chelates; spectral, structural, electrochemical, photoluminescence and computational studies. J Mol Struct 1137:461-475. https://doi.org/10.1016/j.molstruc.2017.02.065

13. Dhar DN, Taploo CL (1982) Schiff bases and their applications. J Sci Ind Res 41(8):501–506.

14. Przybylski P, Huczynski A, Pyta K, Brzezinski B, Bartl F (2009) Biological properties of Schiff bases and azo derivatives of phenols. Curr Org Chem 13(2):124–148. http://dx.doi.org/10.2174/138527209787193774

15. Anacona JR, Noriega N, Camus J (2015) Synthesis, characterization and antibacterial activity of a tridentate Schiff base derived from cephalothin and sulfadiazine, and its transition metal complexes. Spectrochim Acta Part A Mol Biomol Spectrosc 137:16-22. https://doi.org/10.1016/j.saa.2014.07.091

16. Azam M, Wabaidur SM, Haque MN, Khan Z, Al-Resayes SI, Al-Foudhily KA, Soo MI, Trzesowska-Kruszynska A, Kruszynski R (2019) Structural and biological evaluation of a platinum complex as a potential anti-neurodegenerative agent. Inorg Chim Acta 490:235-239. https://doi.org/10.1016/j.ica.2019.03.027

17. Bringmann G, Dreyer M, Faber JH, Dalsgaard PW, Staerk D, Jaroszewski JW, Ndangalasi H, Mbago F, Brun R, Christensen SB (2004) Ancistrotanzanine C and related 5,1′ and 7,3′-coupled naphthylisoquinoline alkaloids from Ancistrocladus tanzaniensis. J Nat Prod 67(5):743–748. https://doi.org/10.1021/np0340549

18. de Souza AO, Galetti FCS, Silva CL, Bicalho B, Parma MM, Fonseca SF, Marsaioli AJ, et al. (2007) Antimycobacterial and cytotoxicity activity of synthetic and natural compounds. Quim Nova 2007;30(7):1563–1566. https://doi.org/10.1590/S0100-40422007000700012

19. Guo Z, Xing R, Liu S, Zhong Z, Ji X, Wang L, Li P (2007) Antifungal properties of Schiff bases of chitosan, N-substituted chitosan and quaternized chitosan. Carbohydr Res 342(10):1329–1332. https://doi.org/10.1016/j.carres.2007.04.006

20. Siegel RL, Miller KD, Jemal A (2016) Cancer Statistics. CA Cancer J Clin 66:7-30. https://doi.org/10.3322/caac.21332

21. a) Czarnomysy R, Surazynski A, Muszynska A, Gornowicz A, Bielawska A, Bielawski K (2018) A novel series of pyrazole-platinum(II) complexes as potential anti-cancer agents that induce cell cycle arrest and apoptosis in breast cancer cells. J Enzym Inhib Med Chem 33:1006-1023. https://doi.org/10.1080/14756366.2018.1471687;
b) Kachalaki S, Ebrahimi M, Khosroshahi L, Mohammadinejad S, Baradaran B (2016) Cancer chemoresistance; biochemical and molecular aspects: a brief overview. Eur J Pharmaceut Sci 89:20–30. https://doi.org/10.1016/j.ejps.2016.03.025

22. Tadele KT, Tsega TW (2019) Schiff Bases and their Metal Complexes as Potential Anticancer Candidates: A Review of Recent Works. Anticancer Agents Med Chem 19(15):1786-1795 http://doi: 10.2174/1871520619666190227171716;
b) Matela G (2020) Schiff Bases and Complexes: A Review on Anti-Cancer Activity. Anticancer Agents Med Chem 20(16): 1908-1917.
http://doi: 10.2174/1871520620666200507091207

23. Palanimurugan A, Kulandaisamy A (2018) DNA, in vitro antimicrobial/anticancer activities and biocidal based statistical analysis of Schiff base metal complexes derived from salicylalidene-4-imino-2,3-dimethyl-1-phenyl-3-pyrazolin-5-one and 2-aminothia-zole. J Organomet Chem 861:263-274.https://doi.org/10.1016/j.jorganchem.2018.02.051

24. Biot C, Nosten F, Fraisse L, Ter-Minassian D, Khalife J, Dive D (2011) The antimalarial ferroquine: from bench to clinic. Parasite 18:207-214. https://doi.org/10.1051/parasite/2011183207

25. Monro S, Colón KL, Yin H, Roque J, Konda P, Gujar S, Thummel RP, Lilge L, Cameron CG, McFarland SA (2019) Transition Metal Complexes and Photodynamic Therapy from a Tumor-Centered Approach: Challenges, Opportunities, and Highlights from the Development of TLD1433. Chem Rev 119:797-828.
https://doi.org/10.1021/acs.chemrev.8b00211

26. Zeng L, Gupta P, Chen Y, Wang E (2017) The development of anticancer ruthenium (II) complexes: from single molecule compounds to nanomaterials. Chem Soc Rev 46:5771-5804. https://doi.org/10.1039/C7CS00195A

27. Gasser G (2015) Metal Complexes and Medicine: A Successful Combination. Chimia 69**:**442-446. https://doi.org/10.2533/chimia.2015.442

28. Azam M, Wabaidur SM, Alam M (2021) Design, structural investigations and antimicrobial activity of pyrazole nucleating copper and zinc complexes. Polyhedron 195:114991. https://doi.org/10.1016/j.poly.2020.114991

29. Gulcan M, Özdemir S, Dündar A, Ispir E, Kurtoglu M (2014) Mononuclear Complexes Based on Pyrimidine Ring Azo Schiff-Base Ligand: Synthesis, Characterization, Antioxidant, Antibacterial, and Thermal Investigations. Z AnorgAllg Chem640:1754-1762. https://doi.org/10.1002/zaac.201400078

30. Gopal Reddy NB, Murali Krishna P, Kottam N (2015) Novelmetal-organic photocatalysts : Synthesis, characterization and decomposition of organic dyes. Spectrochim Acta A 137:371-377. https://doi.org/10.1016/j.saa.2014.08.045

31. González-García C, García-Pascual C, Burón R,Calatayud DG, Perles J, Mendiola MA, Elena López-Torres E (2022) Structural variety, fluorescence and photocatalytic activity of dissymmetric thiosemicarbazone complexes. Polyhedron 223:115945. https://doi.org/10.1016/j.poly.2022.115945

32. Ajji Z, Ali AM (2007) Adsorption of methyl violet and brilliant blue onto poly (vinyl alcohol) membranes grafted with N-vinyl imidazole/acrylic acid. Nucl Instrum Meth B. 265:362–365. http://doi: 10.1016/j.nimb.2007.09.004

33. Mahmoodi NM, Arami M (2009) Numerical finite volume modelling of dye decolorization using immobilized titania nanophotocatalysis. Chem Eng J 46(2):189–193. http://doi: 10.1016/j.cej.2008.05.036.

34. Sriram G, Kigga M, Uthappa UT, Rego RM, Thendral V, Kumeria T (2020) Naturally available diatomite and their surface modification for the removal of hazardous dye and metal ions: a review. Adv Colloid Interfac. 282:102198. http://doi: 10.1016/j.cis.2020.102198

35. Sriram G, Uthappa UT, Rego RM, Kigga M, Kumeria T, Jung HY (2020) Ceria decorated porous diatom-xerogel as an effective adsorbent for the efficient removal of Eriochrome Black T. Chemosphere 238:124692. http://doi: 10.1016/j.chemosphere.2019.124692

36. Hong XJ, Liu X, Zhang JB, Lin CL (2014) Two low-dimensional Schiff base copper(I/II) complexes: synthesis, characterization and catalytic activity for degradation of organic dyes. CrystEngComm16:7926-7932.https://doi.org/10.1039/C4CE01207K

37. Li LJ, Yang LK, Chen ZK, Huang YY, Fu B, Du JL (2014) Synthesis and characterization of multifunctional Schiff base and Cu(II) complex: Degradation of organic dyes and an optical property investigation. Inorg ChemCommun50:62-64. https://doi.org/10.1016/j.inoche.2014.10.020

38. Pandey M, Prajapti R, Shukla P, Paredi P, Tsunoji N, Kumar R, Shahabuddin S, Das S, Bandyopadhyay M (2022) Synthesis of novel tetranuclear Ni complex incorporated mesoporous silica for improved photocatalytic degradation of methylene blue in presence of visible light. Polyhedron 228:116161. https://doi.org/10.1016/j.poly.2022.116161

39. Qu Y-H, Yang Y-J, Dong G-Y (2020) Synthesis, structures, and photocatalytic properties of three new nickel(II) coordination polymers containing bis(benzimidazole) ligands with different coordination architectures. Polyhedron 180:114431. https://doi.org/10.1016/j.poly.2020.114431

40. Mandal S, Sarkar M, Denrah S, Bagchi A, Biswas A, Cordes DB, Slawin AMZ, Saha NC (2023) Catalytic and anticancer activity of two new Ni(II) complexes with apyrazole based heterocyclic Schiff-base ligand: Synthesis, spectroscopy and X-ray crystallography. J Mol Struct 1287:135648. https://doi.org/10.1016/j.molstruc.2023.135648

41. CrystalClear-SM *Exper*t v2.1. Rigaku Americas, *The Woodlands, Texas, USA*, and Rigaku Corporation, *Tokyo, Japan*, (2015)

42. CrysAlis*Pro*v1.171.38.46. Rigaku Oxford Diffraction, Rigaku Corporation, *Oxford, U.K.*, (2015)

43. Burla MC, Caliandro R, Camalli M, Carrozzini B, Cascarano GL, De Caro L, Giacovazzo C, Polidori G, Spagna R (2005) SIR2004: an improved tool for crystal structure determination and refinement. J ApplCrystallogr38:381-388. https://doi.org/10.1107/S002188980403225X

44. Sheldrick GM (2015) Crystal structure refinement with SHELXL. Acta Crystallogr Sect C 71:3-8. https://doi.org/10.1107/S2053229614024218

45. CrystalStructure v4.3.0. Rigaku Americas, *The Woodlands, Texas, USA*, and Rigaku Corporation, *Tokyo, Japan*, (2018).

46. Mukherjee P, Gupta A, Chattopadhyay D, Chatterji U (2017) Modulation of SOX2 expression delineates an end-point for paclitaxel-effectiveness in breast cancer stem cells. Sci Rep **7**:9170. https://doi.org/10.1038/s41598-017-08971-2.

47. Mahajan SD, Law WC, Aalinkeel R, Reynolds J, Nair BB, Yong KT, Roy I, Prasad PN, Schwartz SA (2012) Chapter three - Nanoparticle-Mediated Targeted Delivery of Antiretrovirals to the Brain. Methods in Enzymology 509:41-60. https://doi.org/10.1016/B978-0-12-391858-1.00003-4

48. Tor YS, Yazan LS, Foo JB, Wibowo A, Ismail N, Cheah YK, Abdullah R, Ismail M, Ismail IS, Yeap SK (2015) Induction of Apoptosis in MCF-7 Cells via Oxidative Stress Generation, Mitochondria-Dependent and Caspase-Independent Pathway by Ethyl Acetate Extract of *Dillenia suffruticosa* and Its Chemical Profile. PLoS ONE 10(6): e0127441. https://doi.org/10.1371/journal.pone.0127441

49. Janiak C (2000) A critical account on π–π stacking in metal complexes with aromatic nitrogen-containing ligands. Dalton Trans 21:3885-3896. https://doi.org/10.1039/B003010O

50. Zhao Y, Li J, Gu H, Wei D, Xu YC, Fu W, Yu Z (2015) Conformational Preferences of *π*–*π* Stacking Between Ligand and Protein, Analysis Derived from Crystal Structure Data Geometric Preference of *π*–*π* Interaction. Interdiscip Sci Comput LifeSci **7**:211-220. https://doi.org/10.1007/s12539-015-0263-z.

51. Saha NC, Mandal S, Das M, Khatun N, Mitra D, Samanta A, Slawin AMZ, Butcher RJ, Saha R (2014) Synthesis, characterization, X-ray crystallography and antimicrobial activities of new Co(III) and Cu(II) complexes with a pyrazole based Schiff base ligand. Polyhedron 68:122-130. https://doi.org/10.1016/j.poly.2013.10.016

52. Saha NC, Butcher RJ, Chaudhuri S, Saha N (2003) Synthesis and spectroscopic characterisation of cobalt(III) and nickel(II) complexes with 5-methyl-3-formylpyrazole-N(4)-dibutylthiosemicarbazone (HMP_zNBu_2): X-ray crystallography of $[Co(MP_zNBu_2)_2]NO_3 \cdot H_2O$ (I) and $[Ni(HMP_zNBu_2)_2](ClO_4)_2$ (II). Polyhedron 22:383-390 (and references therein). https://doi.org/10.1016/S0277-5387(02)01343-8

53. Konar S, Jana A, Kar SK (2011) Synthesis, crystal structure, spectroscopic and photoluminescence studies of manganese(II), cobalt(II), cadmium(II), zinc(II) and copper(II) complexes with a pyrazole derived Schiff base ligand. Polyhedron 30:2801-2808. https://doi.org/10.1016/j.poly.2011.08.018

54. Aazam ES, EL Husseiny AF, Al-Amri HM (2012) Synthesis and photoluminescent properties of a Schiff-base ligand and its mononuclear Zn(II), Cd(II), Cu(II), Ni(II) and Pd(II) metal complexes. Arab j chem 5:45-53. https://doi.org/10.1016/j.arabjc.2010.07.022

55. Wang Y, Yang ZY (2008) Crystal structure of Ni(II) complex and fluorescence properties of Zn(II) complex with the Schiff base derived from diethenetriamine and PMBP. J Lumin 128:373-376. https://doi.org/10.1016/j.jlumin.2007.09.002

56. Bagihalli GB, Avaji PG, Patil SA, Badami PS (2008) Synthesis, spectral characterization in vitro antibacterial, antifungal and cytotoxic activities of Co(II), Ni(II) and Cu(II) complexes with 1,2,4-triazole Schiff bases. Eur J Med Chem 43:2639-2649. https:// doi:10.1016/j.ejmech.2008.02.013

57. Basak S, Sen S, Banerjee S, Mitra S, Rosair G, Rodriguez MTG (2007) Three new pseudohalide bridged dinuclear Zn(II) Schiff base complexes: Synthesis, crystal

structures and fluorescence studies. Polyhedron 26:5104-5112. https://doi:10.1016/j.poly.2007.07.025

58. Reddy GR, Chennakesavulu SBK (2014) Zeolite encapsulated Ni(II) and Cu(II) complexes with tetradentate N_2O_2 Schiff base ligand: catalytic activity towards oxidation of benzhydrol and degradation of rhodamine-B. J Mater Chem A 2:15598-15610. https://doi.org/10.1039/C4TA01869A

59. Hiskia A, Mylonas A, Papaconstantinou E (2001) Comparison of the photoredox properties of polyoxometallates and semiconducting particles. Chem Soc Rev 30:62-69. https://doi.org/10.1039/A905675K

60. Patricio C, Yosselin H, Walter R, Jonathan C, Ivan B, Rodrigo A (2020) Synthesis, characterization, X-ray structure, electrochemistry, photocatalytic activity and DFT studies of heterotrinuclear Ni(II), Pd(II) and Zn(II) complexes containing a formyl-ferrocene thiosemicarbazone ligand. Appl Organo met Chem e5974:1. https://doi.org/10.1002/aoc.5974

61. Kang W, Zhong W, Li C, Xia F, Wu Y, Prakash O, Kumar A, Sakiyama H, Muddassir M (2022) Photocatalytic properties of two new isostructural cobalt(II) and nickel(II) complexes having terphenyl-3,3″,4,4″-teteacarboxylic acid. Polyhedron 228**:**116158. https://doi.org/10.1016/j.poly.2022.116158

62. Wang H, Meng X, Fan C, Fan Y, Bi C (2016) Synthesis, crystal structure, DFT study and photocatalytic property of a new Ni(II) complex of a symmetric N_2O_4-donor bis-Schiff base ligand. J Mol Struct 1107:25-30. https://doi.org/10.1016/j.molstruc.2015.11.035

CAPTIONS TO THE FIGURES:

Fig. 1 View of the molecular structure of **I** showing few of the potential hydrogen bonding and π…π stacking interactions observed in the molecule.

Fig. 2 View of the molecular structure of **II** showing few of the potential hydrogen bonding and π…π stacking interactions observed in the molecule.

Fig. 3 Fluorescence spectra of the ligand and the complexes in MeOH; [MPAFA] (**L**), $[Co(MPAFA)_3].2Br.2H_2O$ (**I**) and $[Ni(MPAFA)_3].2Br.2H_2O$ (**II**)

Fig. 4 IC_{50} values of **L**, **I** and **II** on HEK293 cells and human breast cancer cell line MCF7 upon 24 hours of treatment

Fig. 5 Fluorescence microscopy images of treated and untreated MCF7 cells acquired from DCFDA assay and bar diagrammatic depiction of the fluorescence intensity conforming to the level of ROS generation upon 24 hours of treatment with **L**, **I** and **II**

Fig.6 The absorption spectra of the MB solutions during the degradation reaction under UV light irradiation in the presence of **L**

Fig.7 The absorption spectra of the MB solutions during the degradation reaction under UV light irradiation in the presence of **I**

Fig. 8 The absorption spectra of the MB solutions during the degradation reaction under UV light irradiation in the presence of **II**

Fig. 9 (a) Bar diagrammatic representation of the pseudo-first-order plot of MB solution upon 105 minutes of UV light irradiation with the use of **L, I** & **II**; **(b)** Percent of MB dye degradation efficiency of the catalyst **L, I** and **II** upon 105minutes of UV light irradiation

Fig. 10 The pseudo-first-order plot of MB solution under UV light irradiation with the use of **L, I** and **II** and no crystal in the same conditions (**L**: K_1=0.01165 min^{-1}, **I**: K_2=0.01812 min^{-1}, **II**: K_3=0.01454 min^{-1}, without catalyst**:** K_4=0.00149 min^{-1}).

Scheme 1 Synthetic pathway of the complexes

Fig. S1 Packing diagram of complex **I**

Fig. S2 Packing diagram of complex **II**

Fig. S3 Graphical representation of the viability of breast cancer cell MCF7 against different concentrations of compounds **L**, **I** and **II** and their respective linear trend-line equations

Fig. S4 Stability of the compounds **L**, **I** and **II** under UV light irradiation by UV-Vis spectra (shown only charge transfer region)

Fig. S5 Stability of the compounds **L**, **I** and **II** under UV light irradiation by FTIR spectra